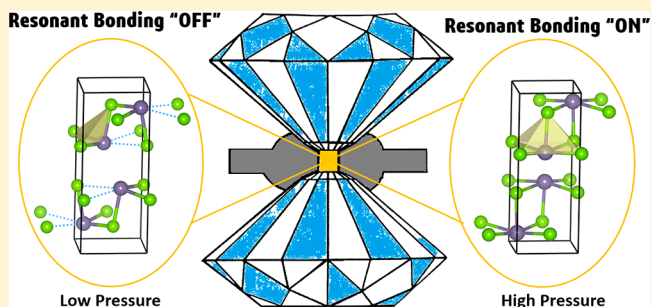


Impact of Pressure on the Resonant Bonding in Chalcogenides

HPSTAR
469-2017Ming Xu,^{*,†,‡,§,¶} Stefan Jakobs,[‡] Riccardo Mazzarello,^{§,||} Ju-Young Cho,[‡] Zhe Yang,^{†,‡} Henning Hollermann,[‡] Dashan Shang,[#] Xiangshui Miao,^{*,†,∇,||} Zhenhai Yu,^{*,†,○,◆} Lin Wang,^{○,¶} and Matthias Wuttig^{‡,⊥,§}[†]School of Optical and Electronic Information, Huazhong University of Science and Technology, Wuhan 430074, China[‡]Institute of Physics (IA) and [§]Institute for Theoretical Solid State Physics, RWTH Aachen University, Aachen 52074, Germany^{||}JARA-FIT and JARA-HPC, and [⊥]JARA-Institut Green IT, Forschungszentrum Jülich GmbH and RWTH Aachen University, Aachen 52056, Germany[#]Beijing National Laboratory for Condensed Matter Physics (BNLCP), Institute of Physics, Chinese Academy of Sciences, Beijing 100190, China[∇]Wuhan National Laboratory for Optoelectronics (WNLO), Wuhan 430074, China[○]Center for High Pressure Science and Technology Advanced Research (HPSTAR), Shanghai 201203, China[◆]School of Physical Science and Technology, ShanghaiTech University, Shanghai 201210, China[¶]High Pressure Synergetic Consortium (HPSynC), Carnegie Institution of Washington, Argonne, Illinois 60439, United States

Supporting Information

ABSTRACT: Resonant bonding has been appreciated as an important feature in some chalcogenides. The establishment of resonant bonding can significantly delocalize the electrons and shrink the band gap, leading to low electrical resistivity and soft optical phonons. Many materials that exhibit this bonding mechanism have applications in phase-change memory and thermoelectric devices. Resonant bonding can be tuned by various means, including thermal excitations and changes in composition. In this work, we manipulate it by applying large hydrostatic-like pressure. Synchrotron X-ray diffraction and density functional theory reveal that the orthorhombic lattice of GeSe appears to become more symmetric and the Born effective charge has significantly increased at high pressure, indicating that resonant bonding has been established in this material. In contrast, the resonant bonding is partially weakened in PbSe at high pressure due to the discontinuity of chemical bonds along a certain lattice direction. By controlling resonant bonding in chalcogenides, we are able to modify the material properties and tailor them for various applications in extreme conditions.



1. INTRODUCTION

The concept of resonance valence bonding (RVB) can be traced back to around 1930, when quantum mechanics was first employed to model the electrons forming chemical bonds.¹ Over many decades, RVB has been discussed intensively in the context of small molecules (e.g., benzene ring), molecular solids (e.g., graphite), and strongly correlated materials (e.g., cuprate compounds^{2,3}). Recently, it has been discovered that a related (but not completely equivalent) bonding mechanism is also prevalent in electron-deficient chalcogenides (i.e., compounds that contain one of the chalcogen elements S, Se, or Te, such as GeTe and Ge–Sb–Te) and materials with closely related electronic structure, such as pure Sb. This bonding mechanism has been called resonant bonding (RB), reminiscent of resonance valence bonding.^{4,5} In rhombohedral Sb and GeTe, for example, each atom is octahedrally coordinated to six neighbors, while the average number of valence electrons for each atom (e.g., three p electrons) is only sufficient to form

three p bonds.^{4–6} Thus, these three p bonds have to be resonant among the six neighbors to stabilize the lattice. RB can delocalize electrons, significantly changing the band gap and the electronic/optical properties. One important application of such a feature is the phase-change memories, which operate between the non-RB amorphous phase and the RB crystalline phase, so that large resistivity and optical contrast can be achieved during phase transformation.^{6–9} Furthermore, the RB is responsible for the softened phonons, entailing extraordinarily low thermal conductivities for some lead/tin chalcogenides, rendering them suitable for thermoelectric applications.^{10–12}

To take advantage of the above virtues of RB, researchers have made many attempts to manipulate it.⁷ The most widely

Received: July 30, 2017

Revised: October 5, 2017

Published: October 24, 2017

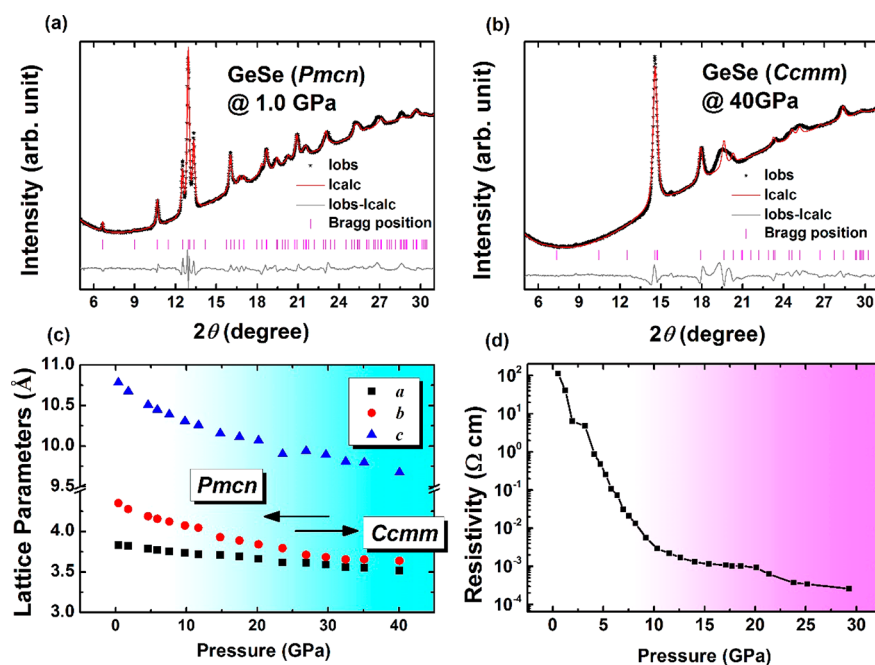


Figure 1. XRD refinement of orthorhombic GeSe with (a) *Pmnc* (GeSe-type) and (b) *Ccmm* (TII-type) symmetries. XRD data were taken at the synchrotron with a wavelength of 0.6199 Å. (c) The evolution of lattice parameters (refined from XRD patterns) against pressure. The structure transition appears to be continuous when GeSe transforms from *Pmnc* to *Ccmm*, which presumably takes place between 25 and 35 GPa. (d) Electrical resistivity of crystalline GeSe as a function of pressure up to 30 GPa, without any abrupt change.

used tool is heating, which has been applied to induce the phase transition in phase-change materials, such that memory cells can switch between RB and non-RB states.⁴ In this work, we use pressure as the tool to control the bonding in several chalcogenides. High-pressure (high-*P*) synchrotron X-ray diffraction (XRD) and resistivity measurements were carried out to monitor the evolution of structure and properties, while density functional theory (DFT) simulations were performed to reveal the electronic structure and bonding nature. The establishment of RB is supported by the significant increase of bond indicators, such as the chemical bond polarizability (Born effective charge) Z^* .^{4,9} Interestingly, the bonding has been changed with hydrostatic-like pressure in PbSe and GeSe, two distinctively different chalcogenides with and without RB, respectively, at ambient conditions. Pressure establishes the RB in GeSe, a widely used electronic material, enabling a continuous structural transition that has been long debated. However, it has an opposite effect on the bonding of the thermoelectric material PbSe.¹⁰ Our work demonstrates that pressure can indeed tune resonant bonding in chalcogenides, offering important implications on the research and design of phase-change memories and thermoelectric devices and providing clues to discover new functionalities that may be related to RB under extreme conditions.^{13–19}

2. METHODS

Samples were prepared and analyzed at the Institute of Physics (IA) of RWTH Aachen University. GeSe films were deposited and annealed at 325 °C for 1 h to ensure that they were fully crystallized. XRD diffraction was then applied to confirm that it was indeed a GeSe-type orthorhombic structure. High-pressure experiments were carried out at the Shanghai Synchrotron Radiation Facility (SSRF) and HPSTAR. We placed GeSe powders obtained from the films into a diamond anvil cell (DAC), together with a ruby chip to determine the pressure²⁰

and silicone oil for pressure transmission. Structural transitions under various pressures (up to 40 GPa) were monitored by the BL15U1 beamline of SSRF with a wavelength of 0.6199 Å. On the other hand, we measured the electrical resistivity of orthorhombic GeSe powders up to 30 GPa in another DAC using the four-point method.²¹

DFT calculations were enabled by the Vienna Ab Initio Simulation Package (VASP) code with supercells containing 32–64 atoms.²² The projector augmented-wave (PAW) method²³ with the generalized gradient approximation (GGA)²⁴ for the exchange–correlation functional was employed. *k*-Point meshes of $16 \times 16 \times 16$ were set for rocksalt and orthorhombic systems. The relaxation behaviors for GeSe and PbSe are remarkably different,^{25–28} e.g., the structure transition of GeSe under high *P* can be accomplished via atomic distortion. Hence, at each pressure step (1% volume reduction for each pressure step between 0 and 50 GPa), we fixed the volume of the cell without fastening the cell shape and ionic positions, and GeSe can accomplish the phase transformation automatically. In contrast, the first-order transition of PbSe is not achievable in density functional theory (DFT) simulations, and both phases (e.g., rocksalt and orthorhombic) of PbSe in the entire pressure range (0–10 GPa) are stable/metastable (the atomic positions and cell shapes of both phases remain almost invariant in this pressure range, even if we allow them to change). The enthalpy changes of the phase transitions are depicted in Figure S1 of the Supporting Information (SI).

Dielectric tensors were determined using density functional perturbation theory with local field effects included in the DFT method.²⁹ Electron localization functions (ELF) were calculated by the equation $ELF = [1 + (D_\sigma/D_\sigma^0)^2]^{-1}$. D_σ denotes the likelihood to find a same-spin electron in the reference region, and D_σ^0 corresponds to the D_σ of a uniform electron gas. Electrons are highly localized when ELF approaches 1 and become more delocalized toward lower values. The ELF

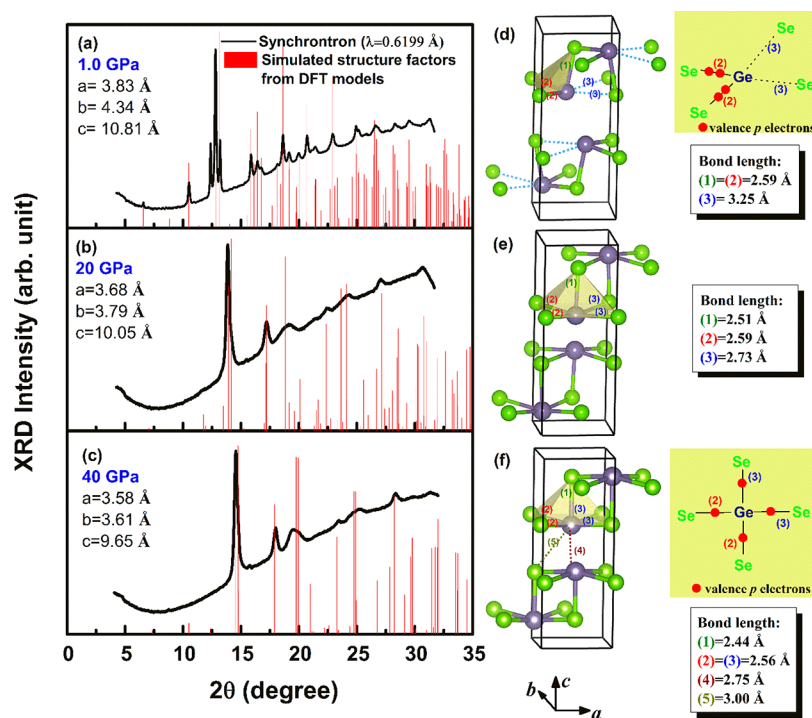


Figure 2. (a–c) Comparison of the experimental and simulated structure factors of GeSe upon increasing pressure. The peak positions of structure factors (red bars) from the DFT simulations are in good agreement with the experiments. The XRD data demonstrate that GeSe gradually transforms from a GeS-type orthorhombic structure to a TII-type one via atomic distortion. The lattice parameters shown in the figures are calculated from simulated models. (d–f) DFT models of GeSe under different pressures. (d) GeSe originally has a GeS-type structure ($Pm\bar{c}n$) at ambient pressure. Each Ge is bonded with three Se atoms with bond lengths of 2.59 Å. The nature of these three bonds is a typical non-RB p-type covalent bonding. (e, f) Under increasing pressure, GeSe gradually evolves into a “pyramid-like” TII-type structure ($Ccmm$) with four equivalent bonds on the base of each pyramid. These four bonds share four p electrons and thus are very likely to be resonant bonds.

approach has been widely used to investigate the chemical bonds because (1) it can easily distinguish the bonding types and (2) compared with the conventional distance cutoff, ELF has better precision in determining when the covalent bond breaks.^{30–34}

3. RESULTS AND DISCUSSION

3.1. Pressure Builds up Resonant Bonding in GeSe.

Synchrotron XRD has been performed on GeSe while applying pressure in a DAC to investigate the structural evolution under high P (Figure 1a,b). At the low- P end, the XRD peaks demonstrate that GeSe has a GeS-type orthorhombic structure (No. 62, $Pm\bar{c}n$).^{35,36} This GeS-type structure is composed of vertex-sharing 3-fold Ge/Se units, as highlighted by the chairlike yellow polygon in Figure 2d. The three bonds (1) and (2) that build each unit share similar bond lengths (2.59 Å) with bond angles of about 91° – 98° , indicating that they are indeed p-type bonds with minor hybridization with s orbitals (see the projected density of states in Figure S3, SI). Besides three nearest atoms, Ge has two second-nearest Se neighbors with a distance of 3.25 Å.

The studies on the high- P phase of GeSe have led to controversies. Bhatia et al.³⁷ discovered an orthorhombic-to-rocksalt transition,³⁸ while Hsueh et al.³⁹ and Onodera et al.⁴⁰ argued that GeSe remains orthorhombic under high pressure. On the computational side, Gashimzade et al. used DFT to study the high-pressure behavior of GeSe and observed an orthorhombic-to-orthorhombic transition at around 29 GPa.⁴¹ By elevating the pressure, we find that some of the XRD peaks smear out and GeSe evolves into another orthorhombic

structure, which appears to be more symmetric. The corresponding XRD patterns from ambient pressure to 40 GPa are plotted in Figure S4 (SI). The phase transition takes place somewhere between 25 and 35 GPa, and at 40 GPa the transition has been completely accomplished. The TII-type orthorhombic structure (No. 63, $Ccmm$) describes this new high- P GeSe phase best. Different from the GeS-type GeSe, the TII-type structure consists of edge-sharing, 5-fold pyramid-like Ge atoms. The transition between these two structures is induced by the distortion of Ge atoms toward the second-nearest Se neighbors, i.e., the long-distance Ge–Se pairs (initially 3.25 Å) have been gradually compressed. The experimental lattice parameters are plotted against pressure in Figure 1c (for more details, see Figure S2, SI), showing that the structure transition is indeed continuous. Further evidence for this continuous phase transition comes from the measurement of the resistivity at elevated pressure, which does not show any abrupt changes up to 30 GPa (Figure 1d).

Consistent with experiments, we find in DFT simulations that the “long bonds” (3) are gradually compressed and eventually become equivalent to the short bonds (2); see Figure 2. The four bonds forming the base of a “square pyramid” have the same bond length and nearly 90° bond angle. However, the total number of valence electrons fails to fit the number of bonds according to “traditional” bonding theory (i.e., each covalent bond is formed by an electron pair). Since s and d electrons do not participate in the bonding (Figure S3, SI) and two p electrons are exclusively owned by bond (1), there are only four valence electrons left over to fill four bonds on the pyramid bottom. Hence, the most probable way to form

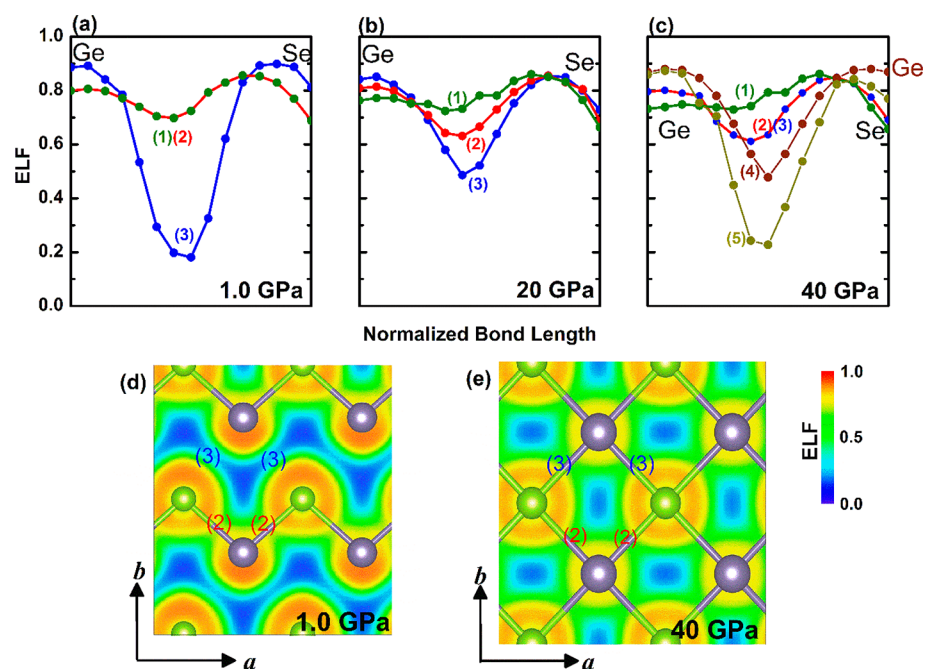


Figure 3. Electron localization functions (ELF) for the Ge–Se bonds under different pressures. ELF toward 1 indicates a high localization of electrons. The numbers in parentheses refer to the bonds marked in Figure 2. (a) At low pressure, electrons are highly localized among three p bonds, while sparsely distributed between the “long bonds”. However, (b) these “long bonds” are gradually compressed and (c) at 40 GPa, they become equivalent (regarding the bond length and ELF) to the short bonds on the pyramid bases, forming 2-D resonant bonds. (d, e) The ELF contours confirm the evolution of Ge–Se bonds from nonresonant bonding to resonant bonding in a – b planes upon compression.

such half-filled valence bonds is the resonance of bonds,⁴ in which each two-electron p bond is split into (or resonant between) two collinear bonds, so that four p electrons can form four bonds between five atomic centers, as depicted in Figure 2f.

Unlike covalent bonds, the formation of ionic bonds normally does not require “electron pairs”, and atoms are adhered by the attractive force between anions and cations (in this case, RB is not required in such “pyramid” clusters). Thus, the primary challenge to verify the establishment of RB is to confirm that these four bonds are not typical ionic bonds. To this end, we calculated the ELF (details are described in the Method section) for Ge–Se bonds under different pressures, because the localization of electrons differs prominently in different bonding types (e.g., in covalent bonds the valence electrons are distributed between two atoms, but they are localized only near anions in ionic solids). The RB-type bonding has salient differences from the non-RB bonding, e.g., the former contains more delocalized electrons, which may entail slightly lower ELF. Nevertheless, the shape of its ELF profile still shows partial localization of the electrons around and between paired atoms, contrary to metallic bonding, wherein electrons are completely delocalized.

Figure 3 shows the ELF profiles of Ge–Se bonds in different GeSe phases. To calculate these bonding profiles, we projected the ELF matrix into the real-space orthorhombic boxes and collected the ELF points near each bond. The core regions in which DFT finds no valence electrons have been left out. The distance cutoff to identify the “bonds” has been set to 3.3 Å, so that even the second nearest Ge–Se pairs—the “long bonds” (3)—can be included in the ELF profiles. In Figure 3a, the ELF drops to 0.2 in the middle of such long bonds, demonstrating that the covalent bonds fail to form because the long Ge–Se pairs are separated by a “vacuum” space barely containing

valence electrons. This vacuum area is also discernible in the ELF contour map in Figure 3d, where the blue regions indicate the low density of localized electrons.

The hydrostatic pressure slightly shortens the vertical bonds (1) and barely changes the bond length of horizontal bonds (2). Yet, the long bonds (3) have been significantly compressed, driving the low- P GeS-type structure into a more symmetric TII-type one. As shown in Figure 2f, the high- P product is composed of the pyramidal units with four equivalent bonds at the base. While the atomic models only demonstrate that these four bonds have the same bond length, the ELF profiles in Figure 3c,e show that electrons are also uniformly distributed between them, which can be explained by the formation of RB. It is noted that, in the low- P GeSe, the interaction between different layers is relatively weak and can even be considered as a van der Waals interaction (the shortest interatomic distance separated by these gaps is larger than 3.3 Å). However, pressure can significantly compress these gaps, shortening the distance between atoms in different layers. At 40 GPa, the interlayer Ge–Ge pairs (4) and Ge–Se pairs (5) have distances of 2.75 and 3.00 Å (Figure 2f). Such small spacing enhances the interaction between layers, but it is still not close enough to form covalent-like bonds. This can be seen from Figure 3c showing that the atomic pairs (4) and (5) have low ELF values of 0.49 and 0.21 in the middle, obviously smaller than that in bonds (1), around 0.80. Hence, the electrons are mostly localized in bonds (1), forming regular p bonds, and RB is unlikely to extend across the gaps in the c direction. Therefore, resonant bonds are only formed in the a – b planes, i.e., the two-dimensional (2-D) RB is observed in this work.

RB can significantly affect the properties of materials. The reason that phase-change materials can be applied in optical data storage devices is because the amorphous and crystalline phases possess large optical contrast, which can be attributed to

the formation of RB when the glass crystallizes. Such large property contrast stems from the delocalization of electrons that RB induces, significantly reducing the band gap (E_g) and increasing the Born effective charge (Z^*). Using density functional perturbation theory, we are able to determine these properties as a function of pressure. The calculated tensors in an orthorhombic system have zero off-diagonal values, so Table 1 lists E_g and only the diagonal components of Z^* tensors.

Table 1. Calculated Lattice Parameters (with experimental data in parentheses), Band Gaps, Bader Charge (charge transfer in parentheses), and Born Effective Charges Z^* of GeSe under Different Pressures (see Figures S2, S3, and S5 of the SI for more details)

structure (pressure)	GeS-type (1.0 GPa)	GeS-type (20 GPa)	TII-type (40 GPa)
lattice parameters (Å)	$a = 3.83$ (3.83) $b = 4.34$ (4.35) $c = 10.81$ (10.78)	$a = 3.68$ (3.66) $b = 3.79$ (3.84) $c = 10.05$ (10.07)	$a = 3.58$ (3.52) $b = 3.61$ (3.64) $c = 9.65$ (9.68)
E_g (eV)	0.80	0	0
Bader charge			
Ge	3.22 (+1.78)	2.74 (+2.26)	2.73 (+2.27)
Se	6.78 (-1.78)	7.26 (-2.26)	7.27 (-2.27)
Z^*_{xx}	3.1	7.9	8.8
Z^*_{yy}	2.5	7.1	8.4
Z^*_{zz}	2.5	4.6	5.3

Obviously, the band gap decreases upon compression, but it alone cannot be the signature of RB because most materials experience shrinking E_g under high pressure. Interestingly, Z^* increases drastically and in a manner that relies crucially on directions [Table 1 and Figure S5 (SI)]. Below 40 GPa, the coupling between the interlayer gaps is still weak and the RB fails to form along the c direction, leading to the slowest increment of Z^* in this direction. In contrast, Z^* increases much faster along the a/b direction, probably due to the

compression of “long bonds” (3) and the delocalization of electrons in the a - b layers. Such a fast increase should not solely originate from the shrinking band gap, and hence, the RB must be at play. The large values of this quantity in the a/b direction provide further evidence for the formation of 2-D RB at high pressure.

One may argue that the rapid rising of Z^* should stem from the large increase of ionicity of bonds upon compression.⁴² However, the increasing ionicity normally opens the band gap, which contradicts with our high- P findings (Table 1). The Bader charge clearly demonstrates that there is no significant change of the charge transfer between Ge and Se, particularly by comparing GeSe at 20 and 40 GPa. Hence, there is no sufficient evidence showing that the bonds become significantly more ionic under high P .

3.2. Pressure Partially Weakens Resonant Bonding in PbSe. Now we look into an opposite case in which pressure partially weakens RB. It is well-known that a large number of rocksalt or distorted rocksalt (rhombohedral) chalcogenides present RB at ambient pressure, such as cubic $\text{Ge}_2\text{Sb}_2\text{Te}_5$ (c -GST), rhombohedral GeTe, and cubic SnTe, PbTe, and PbSe.¹⁰ However, the symmetry of these lattices can easily be changed by pressure, e.g., c -GST is amorphized at 15 GPa^{34,43–46} and rhombohedral GeTe transforms into a complicated orthorhombic structure at higher pressure.⁴⁷ Here, we pick PbSe as the material in question because it is a widely used thermoelectric material that is isoelectronic (i.e., has an equal number of valence electrons) to GeSe and its phase transition under high pressure has already been well-studied.^{48,49}

At ambient conditions, PbSe has perfect rocksalt structure (No. 225, $Fm\bar{3}m$) with 3-D RB.¹⁰ A new TII-type orthorhombic phase (No. 63, $Cmcm$) emerges at 3–4 GPa,⁴⁸ accompanied by a significant increase of electrical resistance by more than 1 order of magnitude.^{48,49} The difference between the rocksalt structure and TII-type structure can be interpreted as every other two-layer block of the rocksalt phase gliding by $0.25(\bar{a} + \bar{b})$

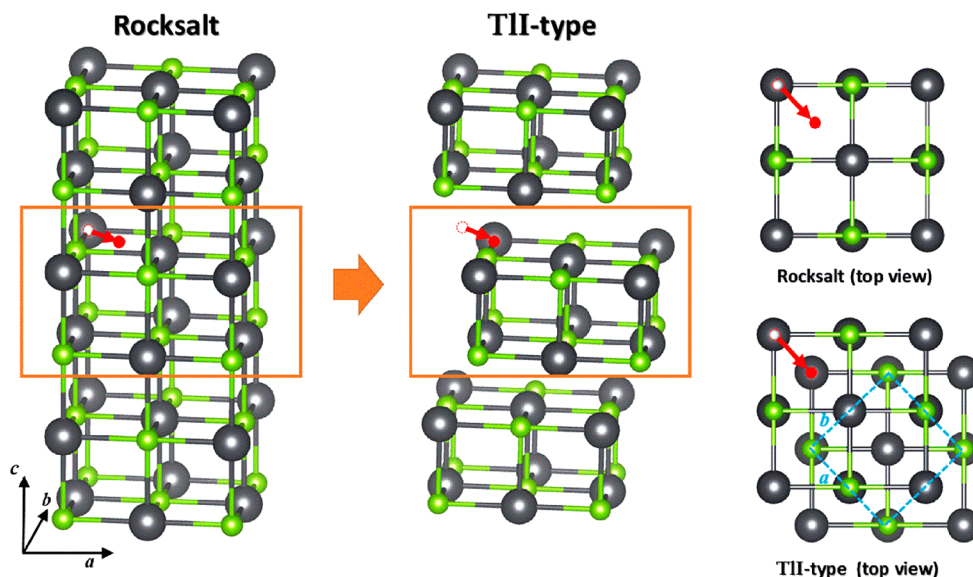


Figure 4. Phase transition from rocksalt structure to TII-type structure can be interpreted as every other two layers sliding by $0.25(\bar{a} + \bar{b})$ along the planar diagonal direction (guided by the red arrows). The blue dashed rectangle marks the unit cell of the TII-type orthorhombic lattice. A slight angular distortion takes place during the transition, and the bonds are also compressed by pressure, so normally a and b are not entirely equivalent in the orthorhombic structure, and hence, the blue dashed rectangle is not a perfect square.

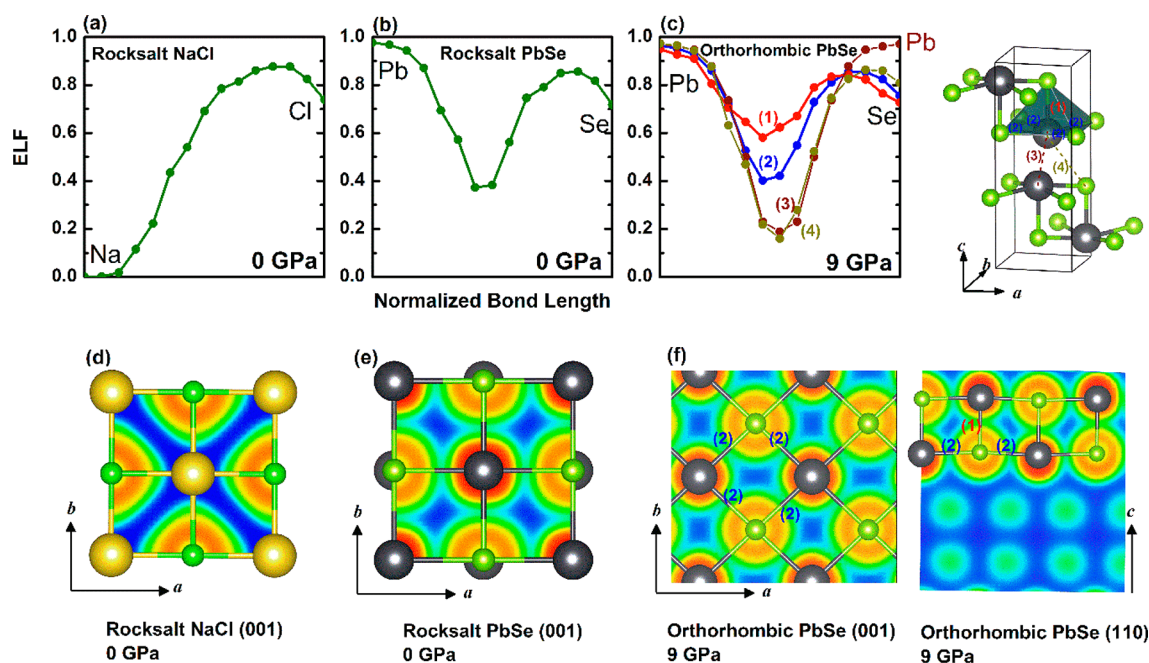


Figure 5. ELF of Pb–Se bonds in low-*P* rocksalt structure and high-*P* orthorhombic structure, in comparison with ionic Na–Cl bonds. (a) NaCl is a typical ionic material with rocksalt structure. The valence electrons are highly localized around Cl ions. (b) In contrast to the ionic Na–Cl bonds, the rocksalt PbSe shows evidence of nonionic bonding. The six undistorted equivalent bonds around each atom share six valence *p* electrons, entailing well-defined 3-D resonant bonding. (c) PbSe undergoes a phase transition from rocksalt to TII-type orthorhombic structure at around 3–4 GPa. Similar to GeSe at high pressure, this new orthorhombic PbSe phase exhibits resonant bonding only in the *a*–*b* plane. Along the *c* direction, the resonant bonds are intercepted by interlayer gaps. (d–f) The ELF contours offer intuitive views of the bonding nature.

\vec{b}) along the planar diagonal direction (Figure 4). We studied these two phases using the DFT method, and their ELF profiles are plotted in Figure 5.

Akin to the GeSe case, the most important challenge is to prove that Pb–Se bonds are mostly nonionic. In order to compare such different bonding natures, we plotted the ELF profile of NaCl (Figure 5a,d), a typical ionic solid. As expected, almost all the electrons are localized around Cl. This electronic configuration of ionic bonds is very different from that observed in rocksalt PbSe (Figure 5b,e), in which electrons are localized around and between both atoms. Hence, this ELF profile indeed indicates that the chalcogenide appears to be not strongly ionic, similar to Ge–Te bonds in GST.³³ The average number of valence *p* electrons in PbSe is three, and once it forms a perfect octahedral configuration, it very probably shows resonant bonding. According to classic chemical bonding theory, the sp^3d^2 hybridization also leads to octahedral configurations, but it requires six valence electrons for each atom, and thus, it is unlikely to occur in the PbSe system.

The medium pressure (3–4 GPa) can turn the rocksalt PbSe into a TII-type structure. Same as GeSe at high pressure, this new PbSe phase is composed of square pyramidal units. As seen from Figure 5c,d, such a structural unit enables the resonant bonding in the *a*–*b* planes due to the uniform covalent bonds (2) and (3), but intercepts the covalent bonds along the *c* direction, as identified from the large difference of ELF profiles between bond (1) and bonds (4) and (5). In this regard, pressure has weakened the RB along the *c* direction and downgraded PbSe from a 3-D RB system to a 2-D one.

Even though RB along the *c* direction is weakened, the one in the *a*–*b* planes appears to be enhanced. One can draw such a conclusion from many aspects: (1) Pressure densifies the material, compressing the Pb–Se bonds and strengthening the

chemical interaction. The DFT-calculated Pb–Se bond length in the rocksalt structure is 3.10 Å, and it splits into 2.80 Å [bond (1)] and 2.98 Å [resonant bonds (2)] in the TII-type structure at 9 GPa, both shorter than the initial length. (2) The shortening of bonds leads to more-localized electrons, as seen by comparing ELF in parts b and c of Figure 5. (3) The calculated Z^* in Table 2 demonstrates that in the *a*–*b* plane RB

Table 2. Calculated Lattice Parameters, Band Gaps, Bader Charge (charge transfer in parentheses), and Born Effective Charges Z^* of PbSe under Different Pressures (see Figures S3 and S5 of the SI for more details)

structure (pressure)	rocksalt (0 GPa)	orthorhombic (5 GPa)	orthorhombic (9 GPa)
lattice parameters (Å)	<i>a</i> = 6.20	<i>a</i> = 4.42 <i>b</i> = 4.16 <i>c</i> = 11.52	<i>a</i> = 4.35 <i>b</i> = 4.08 <i>c</i> = 11.22
E_g (eV)	0.44	0.52	0.46
Bader charge			
Pb	2.51 (+2.39)	2.62 (+2.38)	2.89 (+2.11)
Se	7.39 (−2.39)	7.38 (−2.38)	7.11 (−2.11)
Z^*_{xx}		5.5	5.6
Z^*_{yy}	4.9	5.0	5.1
Z^*_{zz}		3.7	4.0

is enhanced, but along the *c* direction it is weakened. The calculated band gap in an orthorhombic structure is larger than that in the low-*P* phase, probably due to the reduction of RB, which is partly responsible for the anomalous increase of electrical resistivity during the rocksalt-to-orthorhombic transition.^{48,49} (4) The change of ionicity is not responsible for the increase of Z^* along the *a/b* direction, as demonstrated by the

insignificant change of Bader charge transfer on the phase transition.

We performed additional calculations by switching on the spin-orbit coupling for PbSe due to the heavy element lead. The results show a narrower band gap (which is 0.3–0.4 eV smaller than the E_g in Table 2), and consequently, the Born effective charge becomes slightly larger (listed in Table S1 of the SI). Despite of the different computational methods we employed, the trend of data upon pressure appears to be similar: the cubic-to-orthorhombic transition opens up the band gap, enhancing the Z^* along the a/b directions but weakening it along the c directions. This trend is consistent with the change of the bonding mechanism that involves RB.

GeSe and PbSe are both selenides, but they behave differently under high P . This is because their structures and bonding nature differ greatly. GeSe forms short covalent and long “van der Waals” bonds, and once subjected to pressure, the weak long bonds will act as “buffer zones” to be compressed first. Hence, the orthorhombic structure is sustainable even at very high P . In contrast, the rocksalt PbSe is formed by rigid 3-D resonant bonds, and a slight compression of these Pb–Se bonds can easily break the lattice. This is the reason why the transition pressures for GeSe and PbSe are very different, even if they are both selenides.

3.3. Conclusion and Perspective. The formation of RB in chalcogenides is very demanding: the p bonds should be neither too ionic nor too hybridized.^{5,50} At ambient pressure, the relatively strong covalent Ge–Se bonds, which are more hybridized than those in RB materials such as Ge–Te bonds,⁵⁰ forbid the formation of RB in the GeS-type GeSe, leaving three ordinary covalent bonds for each atom. In contrast, the combination of moderate hybridization and ionicity of Pb–Se bonds has enabled rather isotropic 3-D RB in the rocksalt PbSe. However, high pressure drives both materials into the new TII-type orthorhombic structure (the transition pressure of GeSe is between 25 and 35 GPa and that of PbSe is at 3–4 GPa), significantly altering the property of bonds. This TII-type structure is composed of square pyramidal units with four resonant bonds on each quadrilateral base. Some valence electrons are delocalized on these layers due to the RB, which, however, fails to form along the c direction (perpendicular to the layered planes). Hence, the pressure establishes the RB in GeSe but downgrades it in PbSe. By studying these two prototypical materials, we demonstrate that pressure can indeed control the RB and tailor the RB-related properties. Other chalcogenides that undergo similar structural transitions at high pressure⁵¹ may also experience similar phenomena, i.e., establishing or weakening RB. The results may guide researchers to discover and design new memory, thermo-electric, and other functional materials under extreme conditions.

■ ASSOCIATED CONTENT

Supporting Information

The Supporting Information is available free of charge on the ACS Publications website at DOI: 10.1021/acs.jpcc.7b07546.

Figures S1–S5 and Table S1 (PDF)

■ AUTHOR INFORMATION

Corresponding Authors

*M.X. e-mail: mxu@hust.edu.cn.

*X.M. e-mail: miaoxs@hust.edu.cn.

*Z.Y. e-mail: yuzhh@shanghaitech.edu.cn.

ORCID

Ming Xu: 0000-0002-2730-283X

Xiangshui Miao: 0000-0002-6801-2601

Matthias Wuttig: 0000-0003-1498-1025

Author Contributions

The manuscript was written through contributions of all authors. All authors have given approval to the final version of the manuscript.

Notes

The authors declare no competing financial interest.

■ ACKNOWLEDGMENTS

The authors would like to thank Shanghai Synchrotron Radiation Facility (SSRF) for the use of the facilities. This work was partially supported through National Key Research and Development Plan of China (Grant No. 2017YFB0701700 “Materials Genome Engineering”) and Deutsche Forschungsgemeinschaft (SFB 917 “Nanoswitches”). Computational resources were granted by JARA-HPC under the project JARA0143. M.W. acknowledges funding by an ERC Advanced Grant (Grant No. 340698 “Disorder control”). M.X. and J.-Y.C. acknowledge the Alexander von Humboldt Foundation. M.X. acknowledges the Natural Science Foundation of China (NSFC, Grant No. 51772113). X.M. acknowledges the NSFC (Grant No. 61306005, 61474052). L.W. acknowledges the NSFC (Grant No. 11004072) and the Program for New Century Excellent Talents in University (NCET-10-0444). Z.Y. and L.W. acknowledge the support of NSAF (Grant No. U1530402).

■ REFERENCES

- (1) Pauling, L. *The Nature of the Chemical Bond*; Cornell University Press: Ithaca, NY, 1939.
- (2) Anderson, P. W. The Resonating Valence Bond State in La_2CuO_4 and Superconductivity. *Science* **1987**, *235*, 1196–1198.
- (3) Norman, M. R. Cuprates—An Overview. *J. Supercond. Novel Magn.* **2012**, *25*, 2131–2134.
- (4) Shportko, K.; Kremers, S.; Woda, M.; Lencer, D.; Robertson, J.; Wuttig, M. Resonant Bonding in Crystalline Phase-Change Materials. *Nat. Mater.* **2008**, *7*, 653–658.
- (5) Littlewood, P. B. The Crystal Structure of IV–VI Compounds. I. Classification and Description. *J. Phys. C: Solid State Phys.* **1980**, *13*, 4855.
- (6) Wuttig, M. Phase Change Materials: The Importance of Resonance Bonding. *Phys. Status Solidi B* **2009**, *246*, 1820–1825.
- (7) Lencer, D.; Salinga, M.; Wuttig, M. Design Rules for Phase-Change Materials in Data Storage Applications. *Adv. Mater.* **2011**, *23*, 2030–2058.
- (8) Simpson, R. E.; Fons, P.; Kolobov, A. V.; Fukaya, T.; Krbal, M.; Yagi, T.; Tominaga, J. Interfacial Phase-Change Memory. *Nat. Nanotechnol.* **2011**, *6*, 501–505.
- (9) Huang, B.; Robertson, J. Bonding Origin of Optical Contrast in Phase-Change Memory Materials. *Phys. Rev. B: Condens. Matter Mater. Phys.* **2010**, *81*, 081204R.
- (10) Lee, S.; Esfarjani, K.; Luo, T.; Zhou, J.; Tian, Z.; Chen, G. Resonant Bonding Leads to Low Lattice Thermal Conductivity. *Nat. Commun.* **2014**, *5*, 3525.
- (11) Matsunaga, T.; et al. Phase-Change Materials: Vibrational Softening upon Crystallization and Its Impact on Thermal Properties. *Adv. Funct. Mater.* **2011**, *21*, 2232–2239.
- (12) Yan, J.; et al. Pressure-Driven Semiconducting-Semimetallic Transition in SnSe. *Phys. Chem. Chem. Phys.* **2016**, *18*, S012–S018.

- (13) Siegrist, T.; Jost, P.; Volker, H.; Woda, M.; Merkelbach, P.; Schlockermann, C.; Wuttig, M. Disorder-induced localization in crystalline phase-change materials. *Nat. Mater.* **2011**, *10*, 202–208.
- (14) Zhang, W.; Thiess, A.; Zalden, P.; Zeller, R.; Dederichs, P. H.; Raty, J. Y.; Wuttig, M.; Blugel, S.; Mazzarello, R. Role of Vacancies in Metal-Insulator Transitions of Crystalline Phase-Change Materials. *Nat. Mater.* **2012**, *11*, 952–956.
- (15) Xu, M.; Zhang, W.; Mazzarello, R.; Wuttig, M. Disorder Control in a Phase-Change Material GeSb₂Te₄ Using High Pressure. *Advanced Science* **2015**, *2*, 1500117.
- (16) Allen, P. B.; Cohen, M. L. Carrier-Concentration-Dependent Superconductivity in SnTe and GeTe. *Phys. Rev.* **1969**, *177*, 704–706.
- (17) Li, C. W.; Hong, J.; May, A. F.; Bansal, D.; Chi, S.; Hong, T.; Ehlers, G.; Delaire, O. Orbital-Driven Giant Phonon Anharmonicity in SnSe. *Nat. Phys.* **2015**, *11*, 1063–1069.
- (18) Hsieh, D.; Xia, Y.; Qian, D.; Wray, L.; Meier, F.; Dil, J. H.; Osterwalder, J.; Patthey, L.; Fedorov, A. V.; Lin, H.; Bansil, A.; Grauer, D.; Hor, Y. S.; Cava, R. J.; Hasan, M. Z. Observation of Time-Reversal-Protected Single-Dirac-Cone Topological-Insulator States in Bi₂Te₃ and Sb₂Te₃. *Phys. Rev. Lett.* **2009**, *103*, 146401.
- (19) Zhang, H.; Liu, C.-X.; Qi, X.-L.; Dai, X.; Fang, Z.; Zhang, S.-C. Topological Insulators in Bi₂Se₃, Bi₂Te₃ and Sb₂Te₃ with a Single Dirac Cone on the Surface. *Nat. Phys.* **2009**, *5*, 438–442.
- (20) Mao, H. K.; Xu, J.; Bell, P. M. Calibration of the Ruby Pressure Gauge to 800-Kbar under Quasi-Hydrostatic Conditions. *J. Geophys. Res.* **1986**, *91*, 4673–4676.
- (21) Xu, M.; Cheng, Y. Q.; Wang, L.; Sheng, H. W.; Meng, Y.; Yang, W. G.; Han, X. D.; Ma, E. Pressure Tunes Electrical Resistivity by Four Orders of Magnitude in Amorphous Ge₂Sb₂Te₅ Phase-Change Memory Alloy. *Proc. Natl. Acad. Sci. U. S. A.* **2012**, *109*, E1055–E1062.
- (22) Kresse, G.; Furthmüller, J. Efficiency of Ab-Initio Total Energy Calculations for Metals and Semiconductors Using a Plane-Wave Basis Set. *Comput. Mater. Sci.* **1996**, *6*, 15–50.
- (23) Blöchl, P. E. Projector augmented-wave method. *Phys. Rev. B: Condens. Matter Mater. Phys.* **1994**, *50*, 17953–17979.
- (24) Perdew, J. P.; Burke, K.; Ernzerhof, M. Generalized Gradient Approximation Made Simple. *Phys. Rev. Lett.* **1996**, *77*, 3865–3868.
- (25) Gupta, S. D.; Jha, P. K. Vibrational and Elastic Properties as a Pointer to Stishovite to CaCl₂ Ferroelastic Phase Transition in RuO₂. *Earth Planet. Sci. Lett.* **2014**, *401*, 31–39.
- (26) Gupta, S. D.; Gupta, S. K.; Jha, P. K.; Ovsyuk, N. N. A first principles lattice dynamics and Raman spectra of the ferroelastic rutile to CaCl₂ phase transition in SnO₂ at high pressure. *J. Raman Spectrosc.* **2013**, *44*, 926–933.
- (27) Karki, B. B.; Warren, M. C.; Stixrude, L.; Ackland, G. J.; Crain, J. Ab Initio Studies of High-Pressure Structural Transformations in Silica. *Phys. Rev. B: Condens. Matter Mater. Phys.* **1997**, *55*, 3465–3471.
- (28) Lukačević, I.; Gupta, S. K.; Jha, P. K.; Kirin, D. Lattice Dynamics and Raman Spectrum of Rutile TiO₂: The Role of Soft Phonon Modes in Pressure Induced Phase Transition. *Mater. Chem. Phys.* **2012**, *137*, 282–289.
- (29) Gajdoš, M.; Hummer, K.; Kresse, G.; Furthmüller, J.; Bechstedt, F. Linear Optical Properties in the Projector-Augmented Wave Methodology. *Phys. Rev. B: Condens. Matter Mater. Phys.* **2006**, *73*, 045112.
- (30) Savin, A.; Nesper, R.; Wengert, S.; Fassler, T. F. ELF: The electron localization function. *Angew. Chem., Int. Ed. Engl.* **1997**, *36*, 1808–1832.
- (31) Becke, A. D.; Edgecombe, K. E. A Simple Measure of Electron Localization in Atomic and Molecular-Systems. *J. Chem. Phys.* **1990**, *92*, 5397–5403.
- (32) Silvi, B.; Savin, A. Classification of Chemical-Bonds Based on Topological Analysis of Electron Localization Functions. *Nature* **1994**, *371*, 683–686.
- (33) Xu, M.; Cheng, Y. Q.; Sheng, H. W.; Ma, E. Nature of Atomic Bonding and Atomic Structure in the Phase-Change Ge₂Sb₂Te₅ Glass. *Phys. Rev. Lett.* **2009**, *103*, 195502.
- (34) Sun, Z. M.; Zhou, J.; Pan, Y. C.; Song, Z. T.; Mao, H. K.; Ahuja, R. Pressure-Induced Reversible Amorphization and an Amorphous-Transition in Ge₂Sb₂Te₅ Phase-Change Memory Material. *Proc. Natl. Acad. Sci. U. S. A.* **2011**, *108*, 10410–10414.
- (35) Makinistian, L.; Albanesi, E. A. Ab Initio Calculations of the Electronic and Optical Properties of Germanium Selenide. *J. Phys.: Condens. Matter* **2007**, *19*, 186211.
- (36) Dias, R. P.; Kim, M.; Yoo, C.-S. Structural Transitions and Metallization in Dense GeS. *Phys. Rev. B: Condens. Matter Mater. Phys.* **2016**, *93*, 104107.
- (37) Bhatia, K. L.; Gosain, D. P.; Parthasarathy, G.; Gopal, E. S. R. Pressure-Induced First-Order Transition in Layered Crystalline Semiconductor GeSe to a Metallic Phase. *Phys. Rev. B: Condens. Matter Mater. Phys.* **1986**, *33*, 1492–1494.
- (38) Deringer, V. L.; Stoffel, R. P.; Dronskowski, R. Vibrational and Thermodynamic Properties of GeSe in the Quasiharmonic Approximation. *Phys. Rev. B: Condens. Matter Mater. Phys.* **2014**, *89*, 094303.
- (39) Hsueh, H. C.; Vass, H.; Clark, S. J.; Ackland, G. J.; Crain, J. High-pressure effects in the layered semiconductor germanium selenide. *Phys. Rev. B: Condens. Matter Mater. Phys.* **1995**, *51*, 16750–16760.
- (40) Onodera, A.; Sakamoto, I.; Fujii, Y.; Mori, N.; Sugai, S. Structural and Electrical Properties of GeSe and GeTe at High Pressure. *Phys. Rev. B: Condens. Matter Mater. Phys.* **1997**, *56*, 7935–7941.
- (41) Gashimzade, F. M.; Guseinova, D. A.; Jahangirli, Z. A.; Mekhtiev, B. G.; Orudzhev, G. S. Effect of Pressure on Phonon Spectra and Elastic Properties of Orthorhombic GeSe. *Phys. Solid State* **2014**, *56*, 761–764.
- (42) Mukhopadhyay, S.; Sun, J.; Subedi, A.; Siegrist, T.; Singh, D. J. Competing Covalent and Ionic Bonding in Ge-Sb-Te Phase Change Materials. *Sci. Rep.* **2016**, *6*, 25981.
- (43) Kolobov, A. V.; Haines, J.; Pradel, A.; Ribes, M.; Fons, P.; Tominaga, J.; Steimer, C.; Aquilanti, G.; Pascarelli, S. Pressure-Induced Amorphization of Quasibinary GeTe-Sb₂Te₃: The Role of Vacancies. *Appl. Phys. Lett.* **2007**, *91*, 021911.
- (44) Xu, M.; Yu, Z.; Wang, L.; Mazzarello, R.; Wuttig, M. Reversing the Resistivity Contrast in the Phase-Change Memory Material GeSb₂Te₄ Using High Pressure. *Advanced Electronic Materials* **2015**, *1*, 1500240.
- (45) Caravati, S.; Bernasconi, M.; Kuhne, T. D.; Krack, M.; Parrinello, M. Unravelling the Mechanism of Pressure Induced Amorphization of Phase Change Materials. *Phys. Rev. Lett.* **2009**, *102*, 205502.
- (46) Kalkan, B.; Sen, S.; Clark, S. M. Nature of Phase Transitions in Crystalline and Amorphous GeTe-Sb₂Te₃ Phase Change Materials. *J. Chem. Phys.* **2011**, *135*, 124510.
- (47) Sun, Z. M.; Zhou, J.; Mao, H. K.; Ahuja, R. Peierls Distortion Mediated Reversible Phase Transition in GeTe Under Pressure. *Proc. Natl. Acad. Sci. U. S. A.* **2012**, *109*, 5948–5952.
- (48) Wang, S.; et al. Revisit of Pressure-Induced Phase Transition in PbSe: Crystal Structure, and Thermoelastic and Electrical Properties. *Inorg. Chem.* **2015**, *54*, 4981–4989.
- (49) Ovsyannikov, S. V.; Shchennikov, V. V.; Kar'kin, A. E.; Goshchitskii, B. N. Phase Transitions in PbSe under Actions of Fast Neutron Bombardment and Pressure. *J. Phys.: Condens. Matter* **2005**, *17*, S3179.
- (50) Lencer, D.; Salinga, M.; Grabowski, B.; Hickel, T.; Neugebauer, J.; Wuttig, M. A Map for Phase-Change Materials. *Nat. Mater.* **2008**, *7*, 972–977.
- (51) Onodera, A.; Fujii, Y.; Sugai, S. Polymorphism and Amorphism at High Pressure. *Physica B+C* **1986**, *139-140*, 240–245.